

Investigations into the characteristics and influences of nonequilibrium evolution

Xiaobing Li,¹ Mingmei Xu,^{1,*} Yanhua Zhang,² Zhiming Li,¹ and Yuanfang Wu^{1,†}

¹*Key Laboratory of Quark and Lepton Physics (MOE) and Institute of Particle Physics,
Central China Normal University, Wuhan 430079, China*

²*Department of physics and electronic engineering, Yuncheng University, Yuncheng 044000, China*

(Dated: August 10, 2021)

Using the three dimensional (3D) Ising model with Metropolis algorithm, we simulate the evolution from nonequilibrium to equilibrium at zero magnetic field near the critical temperature T_c . To quantify the relaxation time of different processes, the average relaxation time is introduced. It is shown that the average relaxation time is related to system size, temperature and initial configuration. The first four cumulants of order parameter during the nonequilibrium evolution are presented. They all deviate from corresponding equilibrium expectations. In particular, the sign of the third and the fourth cumulants could be either positive or negative, depending on the observation time. These features at $T > T_c$ are consistent with the results obtained from dynamical models. At $T < T_c$, the nonequilibrium evolution lasts much longer, and the influence is much larger in comparison with that at $T > T_c$.

I. INTRODUCTION

One goal of current relativistic heavy ion collision experiments is to map the QCD phase diagram as a function of temperature T and baryon chemical potential μ_B . The phase transition from hadron phase to quark-gluon plasma (QGP) is first order at low T and high μ_B . The first order phase transition line ends at a critical point at which the transition is second order. At high T and small μ_B , the hadron phase smoothly transitions to QGP phase [1–4].

To be able to talk about thermodynamic phases, phase transitions, temperatures and so on, the system under consideration must reach equilibrium [5]. Only at equilibrium, variables such as temperature, pressure and entropy density can be defined, and thermodynamic relations between them can be investigated. Therefore, equilibrium is assumed in lattice QCD and various QCD-based models in their calculations of phase transition.

However, in reality, nonequilibrium is inevitable when the system evolves through the QCD critical region. Near the critical point, the relaxation rate approaches zero and a long time is needed for the system to reach equilibrium, which is the well known critical slowing down. As the expanding fireball formed in a heavy ion collision only spends a limited time in the QCD critical region, the critical slowing down prevents the system from reaching equilibrium.

The nonequilibrium evolution through the QCD critical region may influence the critical observables, such as skewness and kurtosis of the order parameter [6–9]. Skewness and kurtosis of nonequilibrium evolution differ in magnitude or in sign from equilibrium expectations. Taking the skewness of net proton for an example, the equilibrium expectations are positive at the freeze-out

point [10–13]. The measured values by STAR experiment are always negative, i.e. below the Poisson baseline [14]. The negative value may be caused by nonequilibrium effect. Therefore, the discovery of the QCD critical point with a solid experimental basis is highly challenging and has attracted a large number of theoretical and experimental interests.

The nonequilibrium evolution through the QCD critical region is usually assumed to start from an initial state at equilibrium [6, 7, 15]. An interesting issue on the fireball is whether thermal equilibrium is achieved in the initial state [16].

The general picture of relativistic heavy ion collisions is the creation of a fireball of extremely high temperature and density. If the collision energy is high enough and the initial state reaches the temperature needed for the deconfinement phase transition, the fireball transforms to a deconfined phase consisting of interacting quarks and gluons. In that case, QGP phase is formed and the system reaches equilibrium [16]. It is also possible that local equilibrium is reached and QGP is formed in droplets. Another possibility is that some collisions in heavy ion experiments do not experience the phase transition, and the system does not reach equilibrium. Therefore, equilibrium, local equilibrium and nonequilibrium are all possible in the initial states.

For the sample of relativistic heavy ion collisions, it is likely that there is a certain proportion of nonequilibrium initial states. How these nonequilibrium initial states influence observables of the whole sample is interesting and worth studying in order to obtain a comprehensive understanding on the nonequilibrium effects.

Dynamical evolution equations, e.g. Langevin dynamics [8, 15] and various relaxational models [6, 7], are usually used in order to describe the relaxation from nonequilibrium to equilibrium and obtain the effects of nonequilibrium in the QCD critical region. The dynamical evolution equations of nonequilibrium systems in Refs. [6, 7] describe the crossover side of the critical point. They incorporate the fluctuation and dissipation.

*Electronic address: xumm@mail.cnu.edu.cn

†Electronic address: wuyf@mail.cnu.edu.cn

The intrinsic thermal fluctuations drive the system constantly out of equilibrium. Dissipative processes balance the impact of fluctuations. Equilibrium is a result of the balance between dissipation and fluctuations. Near a critical point, the fluctuation is significantly enhanced and equilibrium is hard to reach in a limited time.

Equivalently, Monte Carlo simulations of Ising model with Metropolis algorithm also realize the relaxation from nonequilibrium to equilibrium. Algorithms, e.g. Swendsen-Wang algorithm and Wolff algorithm, belong to cluster algorithms which are more suitable for studying thermal properties at equilibrium. Metropolis algorithm has single-spin-flip mechanism corresponding to a relaxation process [17][18], which is more suitable for studying the evolution from nonequilibrium to equilibrium. Starting from a state far from equilibrium, the Ising model can evolve to the equilibrium state spontaneously. After that, the configuration is not fixed. It can still slightly fluctuate around the equilibrium state, similar to detailed balance. Therefore, the simulation of Ising model with Metropolis algorithm is a realization of dynamical equations of relaxation and is also suitable for the exploration of nonequilibrium features.

Moreover, the Monte Carlo simulation of Ising model can be easily extended to the whole region of the phase boundary. It can describe the relaxation process at any positions on the phase diagram. Therefore, the study of nonequilibrium evolution by using Ising model can help us understand the characteristics of nonequilibrium evolution and its influences on observables on both sides of the critical point.

The QCD critical point explored by heavy ion collisions is expected to belong to the 3D Ising universality class [19–22]. Different thermodynamical systems in the same universality class can not be compared quantitatively, their qualitative characteristics should be similar, however. We expect that the nonequilibrium evolution of the 3D Ising model may have some guidance for heavy ion collisions.

This paper is dedicated to two fold. One is the characteristics of nonequilibrium evolution. The other is the influences of nonequilibrium evolution on observables. The paper is organized as follows. Section II gives a short introduction to Ising model and Metropolis algorithm. In Section III, the dependences of average relaxation time on temperature, system size and initial configuration are investigated. Characteristics of nonequilibrium evolution are presented. Section IV presents the time evolution of cumulants of order parameter. Influences of nonequilibrium on observables are discussed. A summary is given in section V.

II. ISING MODEL AND METROPOLIS ALGORITHM

The 3D Ising model considers a three dimensional cubic lattice composed of $N = L^3$ sites, where L is called

the system size. Every site i is occupied by a spin, s_i . The spins can be in one of two states, either spin-up, $s_i = +1$, or spin-down, $s_i = -1$. The state of the system can be represented by a series of spins, i.e.

$$\{s_1, s_2, \dots, s_N\}. \quad (1)$$

A shorthand notation $\{s_i\}$ is used in the following.

The spins at positions i and j interact with one another. For a pair of parallel spins we assign an interaction energy of $-J$, while for a pair of anti-parallel spins we assign an interaction energy of $+J$. Only interactions with the nearest neighbors are considered.

The spins also interact with an external magnetic field H . The total energy of a system of N spins with constant nearest-neighbor interactions J placed in a uniform external field H is

$$E_{\{s_i\}} = -J \sum_{\langle ij \rangle} s_i s_j - H \sum_{i=1}^N s_i, \quad (2)$$

where the notation $\langle ij \rangle$ restricts the sum to run over all the nearest neighbor spins.

Then the partition function is

$$Z(T, H) = \sum_{\{s_i\}} \exp(-E_{\{s_i\}}/k_B T), \quad (3)$$

where k_B is Boltzmann's constant. The free energy is evaluated by

$$F(T, H) = -k_B T \ln Z. \quad (4)$$

The average total magnetization is

$$M = -\left(\frac{\partial F}{\partial H}\right)_T = \left\langle \sum_{i=1}^N s_i \right\rangle, \quad (5)$$

and the per-spin magnetization is

$$m = \frac{1}{N} \sum_{i=1}^N s_i. \quad (6)$$

We here focus on the behavior of the Ising model as a function of temperature T , which defines an energy scale $k_B T$. For temperatures $k_B T \ll J$, the spin-spin interactions are relatively strong, so that the spins tend to align with one another, and $|m|$ is close to unity. This is an ordered phase. For temperatures $k_B T \gg J$, the spin-spin interactions are relatively weak, so that the spins are effectively non-interacting and point up and down randomly, and $|m|$ is close to zero. This is a disordered phase. A phase transition from a high-temperature disordered phase to a low-temperature ordered phase is anticipated which is continuous and called the Curie point. The Curie point is the critical point on the plane of variables T and H . The temperature of the critical point is denoted by T_c .

The value of T_c of the two dimensional Ising model was exactly calculated by Onsager in 1944 [23]. T_c of the 3D Ising model is estimated by the finite size scaling theory and analysis of magnetization distribution. $K_c = J/k_B T_c = 0.2216544$ is obtained [24], which agrees very well with the results obtained from the renormalization group theory [25]. Usually, J and k_B are set to 1, so $T_c = 4.51$, which is used in the following.

Metropolis algorithm was introduced by Nicolas Metropolis and his collaborators in their paper in 1953 [26]. The main steps of Metropolis algorithm in the 3D Ising model are as follows.

(1) Set the temperature T and the number of sites N .

(2) Generate the initial configuration.

Two kinds of initial configuration are usually used. One is random configuration with all spins pointing randomly up or down, while the other one is polarized configuration with all spins pointing in the same direction.

(3) Test a single spin whether flips or not.

Whether a spin is flipped depends on the acceptance probability $A(\mathbf{u} \rightarrow \mathbf{v})$, which is given by

$$A(\mathbf{u} \rightarrow \mathbf{v}) = \begin{cases} e^{-(E_{\mathbf{v}} - E_{\mathbf{u}})/k_B T} & \text{if } E_{\mathbf{v}} - E_{\mathbf{u}} > 0, \\ 1 & \text{otherwise.} \end{cases} \quad (7)$$

\mathbf{u} and \mathbf{v} represent the state of the system before and after flipping this spin.

If $A(\mathbf{u} \rightarrow \mathbf{v}) = 1$, the spin is flipped.

If $A(\mathbf{u} \rightarrow \mathbf{v}) < 1$, a random number r ($0 < r < 1$) is generated. If $A(\mathbf{u} \rightarrow \mathbf{v}) > r$, the spin is flipped. Otherwise, the spin keeps its original state.

The testing of one single spin is called a Monte Carlo step.

(4) When N Monte Carlo steps are completed, every spin in the lattice has been tested for flipping and we say *one sweep* is completed. In this way, the configuration of the system is updated once a sweep.

(5) After evolving enough sweeps, the magnetization approaches a steady value and the system reaches equilibrium. Thermodynamic quantities are usually measured in the equilibrium state.

(6) Change the temperature or the system size and repeat the above steps.

By using Metropolis algorithm, we simulate the evolution of the 3D Ising model from nonequilibrium to equilibrium at vanished external field and obtain samples for the next calculations.

III. CHARACTERISTICS OF NONEQUILIBRIUM EVOLUTION

Starting from an initial configuration, the Ising system can evolve to an equilibrium state of a given temperature spontaneously. This evolution before reaching equilibrium is called the relaxation process, or *nonequilibrium evolution*.

Starting from random configurations, we simulate 5000 evolution processes for each temperature at a system size $L = 60$. Fig. 1(a)-(d) show the time evolution of $|m|$ (the absolute value of m is used because the sign of the magnetization is random at $H = 0$) at four temperatures, i.e. $T/T_c = 0.93, 0.99, 1.00$ and 1.03 , respectively. The first two temperatures are representative values on the first order phase transition line near the critical point. $T/T_c = 1.00$ represents the critical point. $T/T_c = 1.03$ is a representative value on the crossover side. The horizontal axis is time which is defined by the number of sweeps introduced in the forth step of Metropolis algorithm in section II. The red curve and the blue curve are the results of two evolution processes randomly selected from the sample.

In Fig. 1(a), $|m|$ shows an increasing trend at the beginning, and then gets close to a steady value. After that, $|m|$ fluctuates slightly around the steady value. The steady value represents an equilibrium state, and the approaching to the steady value represents the relaxation to equilibrium.

We use μ to denote the steady value, i.e. the equilibrium expectation. When the difference with the equilibrium expectation is considerably larger than the root of the variance at equilibrium $\sigma = \langle (x - \langle x \rangle)^2 \rangle^{1/2}$, the system is far from equilibrium. The period of time from nonequilibrium to equilibrium is called the relaxation time τ_{eq} [27][28]. In our simulation, relaxation time τ_{eq} is estimated by the time when the value of $|m|$ enters the interval $(\mu - \sigma, \mu + \sigma)$, i.e. the band of thermal fluctuations around the equilibrium expectation.

In Fig. 1(a) the steady values of the red curve and the blue curve are the same, but relaxation time of the red curve is much longer than the blue curve. The difference of relaxation time between the red curve and the blue curve is significant at low temperature as Fig. 1(a) shows and seems diminishing at high temperature as Fig. 1(b)-(d) show. In order to show the difference of relaxation time of different evolution processes, the distributions of τ_{eq} are plotted in Fig. 1(e)-(h). For the sake of comparison, the horizontal ordinate of the four figures are set to the same range.

At the temperature $T/T_c = 0.93$, the distribution of τ_{eq} has a long tail, as shown in Fig. 1(e). The long tail means there are a fraction of evolution processes whose relaxation time is very long. When the temperature gets closer to T_c , the distribution gets narrow, as shown in Fig. 1(f). At the critical temperature, the distribution gets wide again, as Fig. 1(g) shows. The number of systems with a long relaxation time increases at the critical

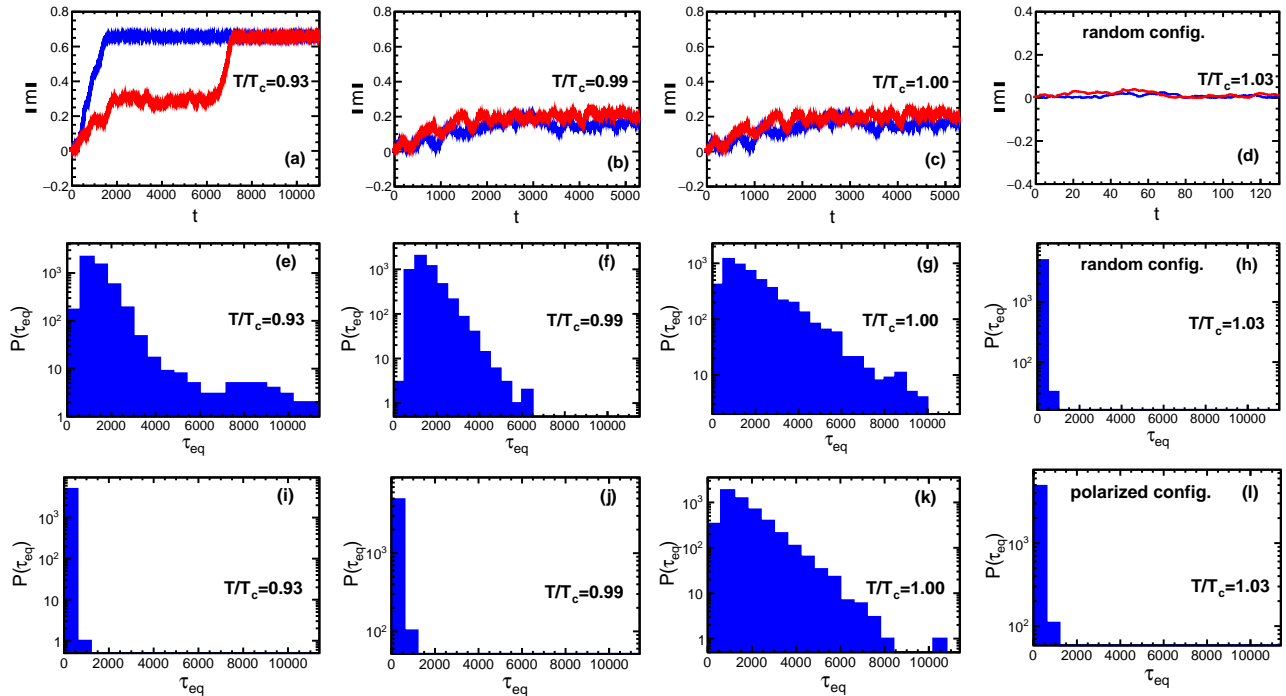


FIG. 1: (a)-(d): The evolution of $|m|$ with time at $L = 60$ for random initial configuration at temperatures $T/T_c = 0.93, 0.99, 1.00$ and 1.03 , respectively. The blue curve and the red curve represent two evolution processes randomly selected from the sample. (e)-(h): The distribution of relaxation time τ_{eq} for random initial configuration at four temperatures. (i)-(l): The distribution of relaxation time τ_{eq} for polarized initial configuration at four temperatures.

temperature. On the crossover side, i.e. $T/T_c = 1.03$, the width of the distribution is the smallest and the distribution is concentrated at very short relaxation time, as Fig. 1(h) shows.

To quantify the relaxation time of different evolution processes, we define the weighted average of relaxation time as

$$\bar{\tau}_{eq} = \frac{\sum_{i=1}^n x_i w_i}{\sum_{i=1}^n w_i}, \quad w_i = \frac{1}{(x_i - \bar{x})^2}, \quad (8)$$

where n is the total number of evolution processes, x_i is relaxation time of the i^{th} evolution process, and \bar{x} is the arithmetical average of relaxation time. At $\bar{\tau}_{eq}$, not all systems are at equilibrium. There is still a proportion of systems in nonequilibrium state. $\bar{\tau}_{eq}$ is introduced to establish a time scale to describe the process of nonequilibrium evolution. As a statistical mean value, $\bar{\tau}_{eq}$ also facilitates a quantitative comparison between different systems.

The weights used in Eq. (8) take very small values on the long tail of the distribution. This procedure effectively reduces the contributions of the tail and makes the weighted average closer to the peak position. The weighted average of relaxation time is called *average relaxation time* in the following.

Generally, the relaxation time depends on the mechanism of dynamic process, the system size, temperature, initial configurations, and so on. In Fig. 2 we system-

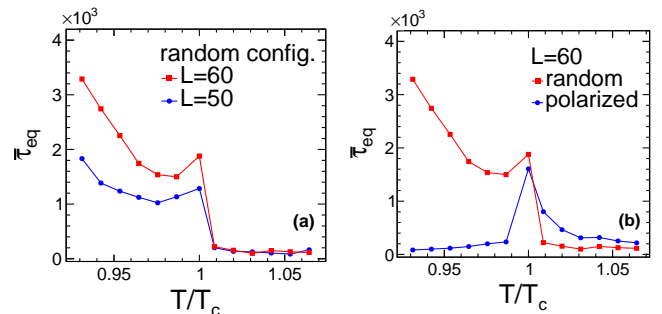


FIG. 2: Average relaxation time $\bar{\tau}_{eq}$ as a function of temperature (a) at system sizes $L = 50$ (blue circles) and 60 (red squares) starting from random initial configuration; (b) for random initial configurations (red squares) and polarized initial configurations (blue circles) at a fixed system size $L = 60$.

atically illustrate how the average relaxation time varies with temperature, the system size and the initial configuration. Fig. 2(a) demonstrates the temperature dependences at two system sizes for a given initial configuration such as a random configuration. Fig. 2(b) demonstrates the temperature dependences for two kinds of initial configuration at a given system size $L = 60$.

In the neighborhood of T_c , the average relaxation time has a peak which increases with the system size, as Fig. 2(a) shows. The peak is expected to diverge at an infinite system size. Fig. 2(b) also shows peaks around the

critical temperature no matter what initial condition is. It is consistent with the expectation from critical slowing down, i.e. the relaxation time diverges at T_c as [29]

$$\tau_{\text{eq}} \propto |T - T_c|^{-\Delta}, \quad (9)$$

where Δ is a critical exponent.

In Fig. 2(a), for a fixed system size, $\bar{\tau}_{\text{eq}}$ shows a decreasing trend with increasing temperature on both sides of T_c except the neighborhood of T_c . This trend originates from that the acceptance probability $A(\mathbf{u} \rightarrow \mathbf{v})$ in Eq. (7) is an increasing function of temperature T . Higher temperature, higher acceptance probability and then shorter relaxation time.

For $T > T_c$, the average relaxation time is weakly dependent on the system size and the initial configuration, as demonstrated in both Fig. 2(a) and (b). No matter what the system size is and what the initial configuration is, the average relaxation time is always short and has a trend towards zero. This is due to larger acceptance probability for higher temperature. With larger acceptance probability, it is easier for the system to change from one configuration to another and hence the relaxation time is extremely short.

In contrary, for $T < T_c$, the average relaxation time has strong dependences on system size and initial configuration. First, Fig. 2(a) demonstrates that the larger system size, the larger average relaxation time. It is natural that larger system needs more time to get equilibrium. Second, Fig. 2(b) demonstrates that the average relaxation time of random configurations is much longer than polarized configurations. This is because random configurations are further from equilibrium state of $T < T_c$, i.e. polarized state. The effect of the two initial configurations is also demonstrated by the distribution of τ_{eq} in the second row and the third row in Fig. 1, respectively. Wide distributions which extend to large τ_{eq} result in large $\bar{\tau}_{\text{eq}}$, while narrow distributions which are concentrated at small τ_{eq} result in small $\bar{\tau}_{\text{eq}}$.

It is natural that the further the initial configuration deviates from the equilibrium state, the longer the relaxation time is. Therefore, on the left side of T_c , random configuration has longer average relaxation time, while on the right side of T_c polarized configuration has longer average relaxation time, as demonstrated in Fig. 2(b).

In order to observe the maximum influences of nonequilibrium, initial configurations that have longer nonequilibrium evolution are selected, i.e. random initial configuration for $T \leq T_c$ and polarized initial configuration for $T > T_c$ are used in the following.

IV. INFLUENCES OF NONEQUILIBRIUM EVOLUTION

In this section the influences of nonequilibrium evolution on observables are demonstrated in two ways, i.e. how observables vary with evolution time and with temperature.

It is shown in last section that the distribution of relaxation time varies with temperature. Even for a fixed temperature and a fixed system size, relaxation time of two simulations is likely to be different, as the red curve and the blue curve show in Fig. 1(a). If measurements are made at a time when not all systems reach thermal equilibrium, there is a certain proportion of nonequilibrium systems in the sample, very similar to the initial states of relativistic heavy ion collisions.

High order cumulants of order parameter are sensitive observables in the search of a critical point. Letting $X = |m|$, $\delta X = |m| - \langle |m| \rangle$, the first four cumulants read

$$C_1 = \langle X \rangle, \quad (10)$$

$$C_2 = \langle (\delta X)^2 \rangle, \quad (11)$$

$$C_3 = \langle (\delta X)^3 \rangle, \quad (12)$$

$$C_4 = \langle (\delta X)^4 \rangle - 3\langle (\delta X)^2 \rangle^2. \quad (13)$$

C_1 is the mean value of order parameter distribution. C_2 is the variance of the distribution. C_3, C_4 are related to skewness and kurtosis, which can quantify non-Gaussianity of the distribution.

Fig. 3 demonstrates how cumulants vary with the evolution time at two given temperatures. The evolution starts at $t = 0$. At $t = 0$, $C_{n=1,2,3,4}$ in Fig. 3(a)-(d) are all zero due to random initial configuration, while C_1 is 1 and $C_{2,3,4}$ are zero due to polarized initial configuration as Fig. 3(e)-(h) show.

The time evolution of C_1 in Fig. 3 (a) and (e) demonstrates a similar behavior with Langevin dynamics, i.e. exponentially approaching the equilibrium value which is the solution of a linear differential equation [30]. Therefore, the single-spin-flip mechanism in Metropolis algorithm equivalently describes the relaxation in Langevin dynamics.

At the temperature on the first order phase transition line, i.e. $T/T_c = 0.99$, C_1 varies monotonously with time until it approaches a steady value, as Fig. 3(a) shows. The steady value is the equilibrium expectation. In Fig. 3(b), C_2 increases first and decreases later, forming a peak during the evolution. In Fig. 3(c) and (d), both C_3 and C_4 experience oscillations before approaching a steady value. The oscillation results in sign changes during the evolution. The sign of C_3 and C_4 can be either positive or negative, depending on the evolution time.

At the temperature on the crossover side, i.e. $T/T_c = 1.01$, the trend of the nonequilibrium evolution of cumulants is similar to that of $T/T_c = 0.99$, as Fig. 3(e)-(h) show. C_1 varies monotonously with time. C_2 experiences nonmonotonic changes before approaching a steady value. C_3 also shows sign change during the evolution, similar to Fig. 3(c). The sign is negative at first and then becomes positive, in contrary to Fig. 3(c). C_4 in Fig. 3(h) also shows sign change, being negative first and then positive, in similar pattern with Fig. 3(d). The sign of C_3 and C_4 can be either positive or negative, depending on the evolution time.

Apart from the trend, the nonequilibrium evolution of

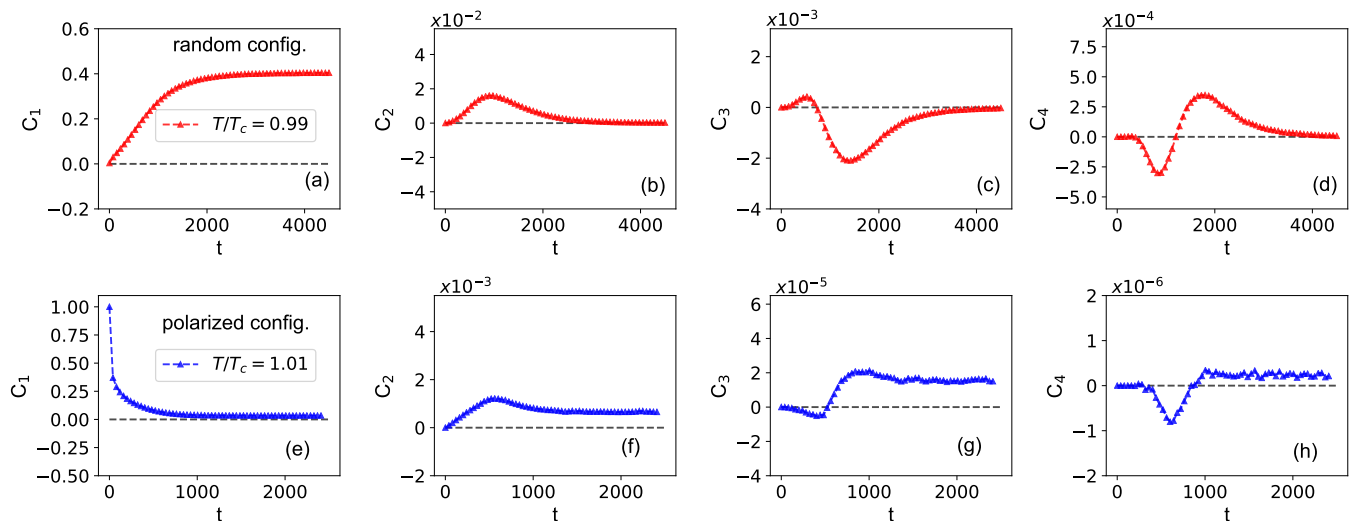


FIG. 3: The time evolution of cumulants of $|m|$ at a given system size $L = 60$ at $T/T_c = 0.99$ (the upper row) and 1.01 (the lower row). Random initial configuration is used at $T/T_c = 0.99$ and polarized initial configuration is used at $T/T_c = 1.01$.

cumulants on both sides of T_c has big differences in two aspects. First, the time needed to approach equilibrium expectations for C_3 is about 4000 at $T/T_c = 0.99$ and is less than 2000 at $T/T_c = 1.01$. The difference is more than twice. That is to say, it is more difficult for systems at $T < T_c$ to achieve equilibrium in the same amount of time. Second, the magnitude of the oscillation in C_3 and C_4 at $T < T_c$ is much larger than that at $T > T_c$, differing about two orders of magnitude. It means that, when systems on both sides of T_c suffer from nonequilibrium effect, systems on the low temperature side deviate further from equilibrium expectations than that on the high temperature side.

Since the sign of C_3 and C_4 during the nonequilibrium evolution depends on the evolution time, two observation times are used as examples to demonstrate in Fig. 4 how observables vary with temperature for a given observation time.

In Fig. 4, cumulants in the upper row are measured at $\bar{\tau}_{\text{eq}}$ and that in the lower row are measured at $3\bar{\tau}_{\text{eq}}$. The equilibrium cumulants denoted by red circles are obtained after 250,000 Monte Carlo sweeps, which ensures that all the systems in the sample reach equilibrium. The blue triangles represent the measured value of cumulants at a given observation time during the nonequilibrium evolution. We call them *nonequilibrium cumulants*.

From the upper row of Fig. 4 we can see that the blue triangles are nearly coincident with the red circles at $T > T_c$ for all $C_{n=1,2,3,4}$. Near T_c , the blue triangles start to deviate from the red circles. It is more clearly seen in the insert map of each figure which focuses on the neighbourhood of T_c . The deviations become larger at $T < T_c$. It means that nonequilibrium cumulants observed at $\bar{\tau}_{\text{eq}}$ are not much different from equilibrium cumulants on the high temperature side. The deviations get larger at low temperature. That is to say, low temperature system is

more largely affected by the nonequilibrium effect.

By comparing different orders of C_n , we find that the deviation of nonequilibrium cumulants from equilibrium cumulants is modest at low order, especially the first cumulant C_1 . Cumulants of higher order have greater deviations from equilibrium fluctuations.

As time goes by, more systems are expected to reach equilibrium, and the impact of nonequilibrium should become smaller. The lower row of Fig. 4 which is measured at a later time $3\bar{\tau}_{\text{eq}}$ indeed shows the expected trend, i.e. more points coincide, including all points at $T > T_c$ and part of points at $T < T_c$. Even in the neighborhood of T_c almost no deviation is seen as shown in the insert map of each figure. Deviations only exist for part of points at $T < T_c$.

At an observation time of $3\bar{\tau}_{\text{eq}}$, nearly all points of C_1 coincide. Deviations of the two colored points in C_2 are modest. Deviations increase drastically in C_3 and C_4 . This proves that relaxation time varies with observables. Relaxation times for higher order cumulants are larger, consistent with expectations [6]. When low order cumulants have reached their equilibrium expectations, high order cumulants may have not reached equilibrium expectations yet.

Observation time of $3\bar{\tau}_{\text{eq}}$ is enough for most temperatures. For $T \lesssim 0.97 T_c$ blue points still deviate from red points as shown in Fig. 4(f)(g)(h). This may be caused by the long tail of the τ_{eq} distribution at low temperature (see Fig. 1(e)).

V. SUMMARY AND DISCUSSION

In this paper we study the nonequilibrium evolution of the three dimensional Ising model at zero external magnetic field and temperatures both on the crossover side

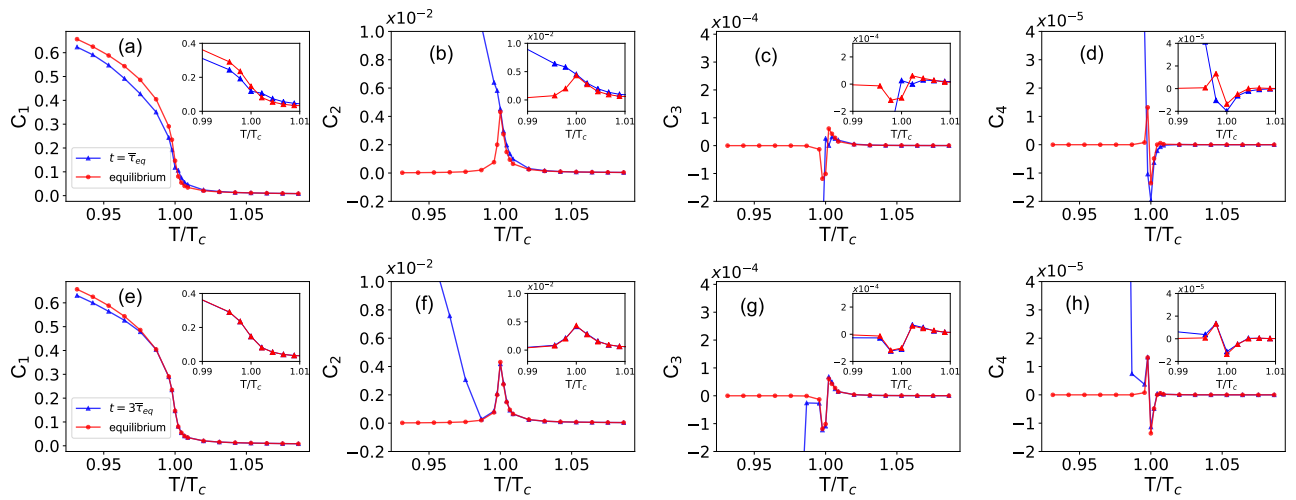


FIG. 4: Nonequilibrium cumulants of $|m|$ at a given system size $L = 60$ measured at $\bar{\tau}_{\text{eq}}$ (the upper row) and $3\bar{\tau}_{\text{eq}}$ (the lower row), respectively. Random initial configuration is used for $T \leq T_c$ and polarized initial configuration is used for $T > T_c$.

and on the first order phase transition line near the critical point.

We firstly introduce the average relaxation time to describe the evolution of systems to the equilibrium. It is found that the average relaxation time depends on the system size. For larger system size, the average relaxation time is longer. The average relaxation time also depends on temperature. In average, the average relaxation time is short at $T > T_c$, almost independent of initial configurations. At $T < T_c$, when selecting configurations that deviate far from the equilibrium state as initial configurations, the average relaxation time is much longer than that of $T > T_c$.

The time evolution of the first four cumulants of order parameter is presented. For both $T < T_c$ and $T > T_c$, C_1 shows a monotonic behavior with time. C_2 shows a peak with time. C_3 and C_4 show oscillations and could be either positive or negative, depending on the observation time, which is consistent with the results of dynamical models [6, 7].

It is also shown that the relaxation time at $T < T_c$ is

much longer than that at $T > T_c$. Therefore, it is easy to approach equilibrium at the crossover side. While on the line of the first order phase transition, the system is more difficult to achieve equilibrium and is more susceptible to nonequilibrium. Moreover, the influence of nonequilibrium on observables on the crossover side is much weaker than that on the line of the first order phase transition.

Quantitatively, these characteristics and influences depend on the model, or algorithm, and the specific system. Nevertheless, basic conclusions should be qualitatively model independent, and therefore should be instructive for exploring the QCD critical point, the crossover region and the phase boundary in relativistic heavy ion collisions.

Acknowledgement

We thank Yi Yin, Huichao Song and Shanjin Wu for interesting discussions. This work is supported in part by the NSFC of China under Grant No. U1732271.

-
- [1] Y. Aoki, G. Endrodi, Z. Fodor, S. D. Katz and K. K. Szabo, *Nature* **443**, 675 (2006).
 - [2] S. Ejiri, *Phys. Rev. D* **78**, 074507 (2008).
 - [3] E. S. Bowman and J. I. Kapusta, *Phys. Rev. C* **79**, 015202 (2009).
 - [4] H. T. Ding, F. Karsch and S. Mukherjee, *Int. J. Mod. Phys. E* **24**, 1530007 (2015)
 - [5] P. Braun-Munzinger, J. Stachel, *Nature* **448**, 302 (2007).
 - [6] S. Mukherjee, R. Venugopalan and Y. Yin, *Phys. Rev. C* **92**, 034912 (2015).
 - [7] M. Nahrgang, M. Bluhm, T. Schafer and S. A. Bass, *Phys. Rev. D* **99**, 116015 (2019).
 - [8] S. Wu, Z. Wu and H. Song, *Phys. Rev. C* **99**, 064902 (2019).
 - [9] K. Rajagopal, G. Ridgway, R. Weller and Y. Yin, *Phys. Rev. D* **102**, 094025 (2020).
 - [10] M. Stephanov, K. Rajagopal and E. Shuryak, *Phys. Rev. Lett.* **81**, 4816 (1998).
 - [11] M. Stephanov, K. Rajagopal and E. Shuryak, *Phys. Rev. D* **60**, 114028 (1999).
 - [12] M. Stephanov, *Phys. Rev. Lett.* **107**, 052301 (2011).
 - [13] M. Asakawa, S. Ejiri and M. Kitazawa, *Phys. Rev. Lett.* **103**, 262301 (2009).
 - [14] J. Adam et al. (STAR Collaboration), *Phys. Rev. Lett.* **126**, 092301 (2021).
 - [15] B. Berdnikov and K. Rajagopal, *Phys. Rev. D* **61**, 105017 (2000).

- [16] J. Adams et al. (STAR Collaboration), Nucl. Phys. A **757**, 102 (2005).
- [17] Cheng-Wei Liu, A. Polkovnikov and A. W. Sandvik, Phys. Rev. B **89**, 054307 (2014).
- [18] M. Acharyya, Phys. Rev. E **56**, 2407 (1997).
- [19] R.D. Pisarski, F. Wilczek, Phys. Rev. D **29**, 338 (1984).
- [20] M. Stephanov, K. Rajagopal, E. Shuryak, Phys. Rev. Lett. **81** 4816 (1998).
- [21] M. Asakawa, J. Phys. G: Nucl. Part. Phys. **36** 064042 (2009).
- [22] P. de Forcrand, O. Philipsen, Phys. Rev. Lett. **105** 152001 (2010).
- [23] L. Onsager, Phys. Rev. **65**, 117 (1944).
- [24] A L Talapov, and H W J. Blöte, J. Phys. A **29**,5727(1996).
- [25] G. S. Pawłcy, R. H. Swendsen, D. J. Wallace and K. G. Wilson, Phys. Rev. B **29**, 4030 (1984).
- [26] N. Metropolis, A. W. Rosenbluth, M. N. Rosenbluth, A. H. Teller, and E. Teller, J. Chem. Phys.
- [27] M E J Newman and G T Barkema. Monte carlo methods in statistical physics[M]. Oxford University Press, 1999.
- [28] Helmut G. K arXiv:0905.1629(2009).
- [29] D. T. Son and M. A. Stephanov, Phys. Rev. D **70**, 056001 (2004).
- [30] Eq. (118.5) in Statistical Physics Part 1, Third edition, L. D. Landau and E. M. Lifshitz, 1980.